Atmos. Chem. Phys., 11, 12887–12900, 2011
www.atmos-chem-phys.net/11/12887/2011/
doi:10.5194/acp-11-12887-2011

Atmospheric Chemistry and Physics

Resolving both entrainment-mixing and number of activated CCN in deep convective clouds

E. Freud[1], **D. Rosenfeld**[1], **and J. R. Kulkarni**[2]

[1]The Department of Atmospheric Sciences, The Hebrew University of Jerusalem, 91904 Jerusalem, Israel
[2]Institute of Tropical Meteorology, Dr. Homi Bhabha Road, Pashan, Pune 411008, India

Received: 24 February 2011 – Published in Atmos. Chem. Phys. Discuss.: 22 March 2011
Revised: 27 November 2011 – Accepted: 1 December 2011 – Published: 20 December 2011

Abstract. The number concentration of activated CCN (N_a) is the most fundamental microphysical property of a convective cloud. It determines the rate of droplet growth with cloud depth and conversion into precipitation-sized particles and affects the radiative properties of the clouds. However, measuring N_a is not always possible, even in the cores of the convective clouds, because entrainment of sub-saturated ambient air deeper into the cloud lowers the concentrations by dilution and may cause partial or total droplet evaporation, depending on whether the mixing is homogeneous or extreme inhomogeneous, respectively.

Here we describe a methodology to derive N_a based on the rate of cloud droplet effective radius (R_e) growth with cloud depth and with respect to the cloud mixing with the entrained ambient air. We use the slope of the tight linear relationship between the adiabatic liquid water mixing ratio and R_e^3 (or R_v^3) to derive an upper limit for N_a assuming extreme inhomogeneous mixing. Then we tune N_a down to find the theoretical relative humidity that the entrained ambient air would have for each horizontal cloud penetration, in case of homogeneous mixing. This allows us to evaluate both the entrainment and mixing process in the vertical dimension in addition to getting a better estimation for N_a.

We found that the derived N_a from the entire profile data is highly correlated with the independent CCN measurements from below cloud base. Moreover, it was found that mixing of sub-saturated ambient air into the cloud at scales of ~100 m and above is inclined towards the extreme inhomogeneous limit, i.e. that the time scale of droplet evaporation is significantly smaller than that for turbulent mixing. This means that ambient air that entrains the cloud is pre-moistened by total evaporation of cloud droplets before it mixes deeper into the clouds where it can hardly change the droplet size distribution, hence R_e remains close to its adiabatic value at any given cloud depth. However, the tendency towards the extreme inhomogeneous mixing appeared to slightly decrease with altitude, possibly due to enhanced turbulence and larger cloud drops aloft.

Quantifying these effects, based on more examples from other projects and high resolution cloud models is essential for improving our understanding of the interactions between the cloud and its environment. These interactions may play an important role in cloud dynamics and microphysics, by affecting cloud depth and droplet size spectra, for example, and may therefore influence the cloud precipitation formation processes.

1 Introduction

Clouds are responsible for two thirds of the planetary albedo and hence play a dominant role in determining the Earth energy budget and the global temperature. Aerosols affect cloud albedo by nucleating larger number of smaller droplets that enhance the light scattering for a given amount of cloud water (Twomey, 1974). According to the IPCC (2007) report, the uncertainty in the aerosol cloud albedo effect, particularly in the anthropogenic aerosol component, dominates the uncertainty of the climate radiative forcing. Aerosols can also alter the cloud coverage and lifetime of both cooling (Albrecht, 1989) and warming (Koren et al., 2010), and significantly affect the precipitation processes and hence the redistribution of heat and energy in the atmosphere (Rosenfeld et al., 2008a). This occurs through the aerosol impacts on precipitation forming processes and the following modification of cloud dynamics. These processes are at least as important and even less understood than the albedo effect which was highlighted as the main source of uncertainty (IPCC, 2007).

Correspondence to: E. Freud
(eyal.freud@mail.huji.ac.il)

Published by Copernicus Publications on behalf of the European Geosciences Union.

Aerosols and clouds are microphysically related through the number of the activated aerosols that serve as cloud condensation nuclei (CCN) and produce cloud droplets. This depends on the sizes, concentrations and chemical properties of the aerosols as well as on the super-saturation that they were exposed to. As long as the droplet concentrations and their surface areas are too small to balance the super-saturation produced by the cooling of the rising saturated air, more CCN will activate into cloud droplets. Stronger updrafts will result in higher droplet concentrations. Even relating the much more common retrievals of aerosol optical depths (AOD) to CCN concentrations at a given super-saturation can be problematic, because the same retrieved AOD can be the result of significantly (orders of magnitude) different CCN concentrations (Andreae, 2009).

The number of activated CCN (henceforth: N_a) into cloud droplets is the most fundamental microphysical property of a convective cloud. It determines the rate of the droplets' growth with cloud depth and in turn their conversion into precipitation-sized particles. It also affects the radiative properties of the clouds as higher concentrations will reduce the droplet sizes for a given amount of cloud water (Twomey, 1974). N_a embodies not only the CCN activation spectra, but also the actual super-saturation that these CCN were exposed to. However, direct measurement of N_a is usually not possible because entrainment of sub-saturated ambient air into the cloud decreases the cloud droplet concentrations by evaporation and dilution. Even the cores of deep convective clouds, where measurements are normally avoided due to the strong vertical motions and icing hazards, are prone to entrainment. This is mainly because of their fairly small horizontal extent and the strong turbulence in and near the convective clouds. Indirect measurements of N_a by satellite and lidar retrievals were previously applied to shallow marine stratiform clouds, with the main assumption that the clouds are composed of nearly adiabatic elements (Bennartz, 2007; Brenguier et al., 2000; Schüller et al., 2003; Snider et al., 2010). These retrievals had large uncertainties and were not always validated with direct measurements. Furthermore, that methodology is not applicable to convective clouds due to a large departure from the assumption that they are close to adiabatic, and also due to the variable cloud top heights and depths at scales smaller than the typical satellite sensor resolution.

Here we introduce a methodology for deriving N_a of convective clouds in a wide range of aerosol and cloud droplet concentrations, and even for diluted clouds. This methodology, presented in Sect. 3, is based on in-situ measurements of the cloud droplet spectra at different levels in clouds. But first we discuss the entrainment-mixing process of sub-saturated ambient air into the cloud in Sect. 2.

2 Entrainment-mixing processes

Typically, as soon as a convective cloud is formed in a super-saturated rising bubble of air, it continues to grow upwards into a layer of sub-saturated air. As long as the cloud is not precipitating and without significant dilution by entrained air, its liquid water content (LWC) is expected to be close to the adiabatic water content (LWC_a[1]). Nearly adiabatic values of LWC are often measured in Stratus (St) and Stratocumulus (Sc) clouds because of their relatively wide extent so that much of their cloud volume does not come into contact with the surrounding sub-saturated air. Convective clouds, however, have a much smaller horizontal dimension and are more turbulent, so that the entrained sub-saturated air from the surroundings of the clouds has a high chance of quickly penetrating deeper into the cloud and reaching its core while lowering LWC by dilution. Barahona and Nenes (2007) developed a parameterization based on the assumption that mixing occurs already at the cloud formation level, which results in a reduction in the number of activated CCN in convective clouds. This is because the entrainment at cloud base lowers the maximum super-saturation that is reached. Morales et al. (2011) showed that this parameterization yields a mean cloud droplet number concentration that is comparable with the numbers measured in convective clouds. The cloud droplets that are exposed to that sub-saturated air will partially or completely evaporate and increase the water vapor partial pressure in the entrained air. The fate of the droplets is determined by the mixing proportions of the cloudy and ambient air, its relative humidity (RH) and the sizes and concentrations of the droplets. Without mixing, precipitation, secondary droplet nucleation and droplet coalescence, the droplet mean volume radius, henceforth R_v, is expected to be equal to R_v in an adiabatic parcel (R_{v_a}), which only depends on N_a and LWC_a (Eq. 1). Again, model and airborne studies reveal that in Sc clouds, R_v and R_{v_a} are quite similar, except for close to the cloud edges, and especially near the top of the cloud where most mixing occurs (e.g. Pawlowska et al., 2000). How exactly mixing and entrainment affect the droplet size distribution (DSD) and R_v is an issue that has been studied for more than three decades and there is still no satisfying answer, specifically in convective clouds. This is because mixing starts with eddies with a length scale of hundreds or even thousands of meters that gradually break into smaller filaments down to the Kolmogorov microscale ($\sim$1 mm in normal atmospheric conditions), where variations in temperature and water vapor fields are homogenized by molecular diffusion. Such scales cannot be explicitly resolved by today's cloud models and standard airborne cloud microphysics instrumentation (Baker et al., 1984; Brenguier, 1993; Lehmann et al., 2009).

[1]The subscript "a" added to LWC, R_v and R_e in this paper stands for "adiabatic" to denote the values of these parameters in an adiabatic air-parcel

Until the late 1970s the research of the entrainment-mixing process was based on the idea that the cloud droplets at any given level are equally exposed to the entrained sub-saturated air, regardless of their specific location in the cloud, and as a result evaporate partially or completely together – what was later described as homogeneous mixing by Baker et al. (1980). In a laboratory study, Latham and Reed (1977) found that concentrations of small droplets become very inhomogeneous after admixture with sub-saturated air, because some of the droplets totally evaporate while others remain unchanged. This finding helped explain some of the discrepancies between earlier calculations and modeling results, and observations in clouds. In their published studies, Baker et al. (1980) and Blyth et al. (1980) prepared the ground for the current research on the effect of mixing and entrainment on cloud droplet spectra. They defined the range of the mixing effect on cloud droplet spectra based on the time scales of droplet evaporation (τ_{evap}) vs. turbulent mixing (τ_{mix}). In the case that $\tau_{evap} \ll \tau_{mix}$ the droplets that border the entrained air bubble or filament will quickly evaporate until the entrained air becomes saturated, so further mixing will decrease the cloud droplet concentration by dilution and will leave the shape of the droplet spectra unchanged. This is referred to as the extreme inhomogeneous case. The other extreme is the homogeneous mixing. It fulfills the condition: $\tau_{evap} \gg \tau_{mix}$. That means that the sub-saturated air will be first fully mixed in the cloud volume, so all droplets will be exposed to the same sub-saturation, and then will partly evaporate until the air becomes saturated again. This will cause the droplet size spectra to shift towards the smaller sizes but the number of droplets will remain the same unless some of the smallest droplets would fully evaporate. In reality though, the ratio between τ_{mix} and τ_{evap}, also called the Damköhler ratio (Dimotakis, 2005), is typically not much smaller or larger than unity. It depends on the mixing scales, which are hard to define, the turbulence, the ambient RH, the droplets' sizes and concentrations etc. (Lehmann et al., 2009).

Figure 1 demonstrates the fundamental differences between the fully homogeneous and extreme inhomogeneous mixing scenarios, as described above. It shows an example of the theoretical relationship between the droplet mean volume radius (R_v) and the adiabatic fraction (AF), which is the ratio between LWC and LWC_a, for the two mixing scenarios. We use typical values for the parameters that affect this relationship to get typical values of R_v. We assume isobaric mixing of cloudy and ambient air that have the same temperature. This figure resembles the mixing diagram shown in Burnet and Brenguier (2007) and the parameters are calculated in the same way, but here we plot AF on the abscissa rather than the normalized number of droplets, because it represents better the amount of entrained air that the adiabatic parcel has been mixed with. How much the droplets will reduce in size in relation to R_{v_a} when exposed to sub-saturated air is determined by the initial water vapor content of the entrained air: the drier it is the smaller the droplets will become upon

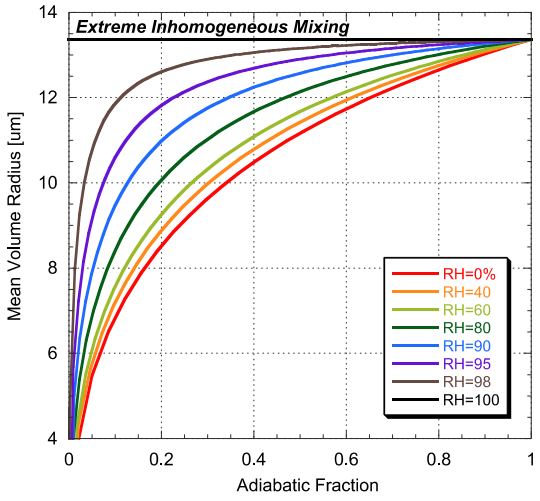

Fig. 1. Mixing diagram: the relationship between the droplet mean volume radius (R_v) and the adiabatic fraction (AF) for fully homogeneous and extreme inhomogeneous mixing events between an adiabatic cloud parcel and entrained non-cloudy air with varying relative humidity (RH) at the mixing level of ∼2200 m above cloud base, where the temperature of the cloudy and entrained air is ∼10 °C and the adiabatic liquid water mixing ratio is 5 g kg^{-1}. The cloud base is at 850 hPa and 20 °C. The concentration of the activated CCN (N_a) is 500 mg^{-1}. It can be seen that entrained air with higher RH results in a smaller dependence of R_v on AF, especially for AF>0.2. When entrained air is saturated (RH = 100 %), or when mixing is extremely inhomogeneous, R_v remains constant.

mixing and saturation of the entrained air, until their mass is not sufficient to saturate the mixed air and they completely evaporate. Mixing with air that is already saturated, or in case of extreme inhomogeneous mixing, R_v will be equal to R_{v_a} for all adiabatic fractions. Figure 1 clearly shows that the R_v vs. AF curve strongly depends on the RH of the entrained air, but this dependence is highly non-linear: at low RH this relationship is almost independent of RH, whereas in high RH this relationship has a strong sensitivity to RH. If the RH of the entrained air is known then the deviation from the homogeneous mixing curve for that RH with respect to the extreme inhomogeneous mixing horizontal line in Fig. 1 can give an indication of the extent of the mixing inhomogeneity. For example, if the ambient RH is 30 %, but the data points plotted on a mixing diagram like Fig. 1 align around the RH = 95 % curve, then this would be a strong indication of mixing tendency towards the inhomogeneous limit.

Generally, it appears in the literature that the observational studies find a clear tendency towards the extreme inhomogeneous mixing (Hill and Choularton, 1985; Paluch, 1986; Bower and Choularton, 1988; Pawlowska et al., 2000; Gerber, 2006) or intermediate features between the homogeneous and inhomogeneous mixing scenarios (Jensen and Baker, 1989; Paluch and Baumgardner, 1989; Morales et al., 2011), although parts of this tendency may be explained by

instrumental artifacts (Burnet and Brenguier, 2007). In an earlier study of ours that analyzed many convective cloud droplet spectra in the Amazon basin (Freud et al., 2008), we also concluded that the mixing process tends towards the extreme inhomogeneous limit, as the droplet effective radii (R_e) did not show a significant dependence on the extent of droplet exposure to entrained air. Our analysis here, looks deeper into the mixing process in a quantitative way, so we are able to use the deviations from the extreme inhomogeneous mixing assumptions to derive a better estimation for N_a, which is the main objective in this study.

3 Methods

The number of activated CCN, N_a, which we aim to derive, is a macro-physical cloud property similar to the precipitation initiation height. It represents a whole cloud or even a cloud domain where aerosol and thermodynamic features do not vary considerably. Therefore it cannot be based on an individual measurement at the cloud droplet probe spatial resolution (typically ~100 m), such as the maximum droplet concentration. This is because a single measurement may have a large uncertainty, be sensitive to processes on a scale too small to represent the entire cloud (e.g. local strong updraft near cloud base) and be affected by the extent of dilution that the measured cloud volume had experienced. Instead, basing the estimation of N_a on many measurements throughout the cloud and at different levels, and using a more robust microphysical property such as R_e or R_v, is expected to be more representative and less prone to the uncertainties of the individual measurements. This is the approach we use here.

The methodology we use to derive N_a is first stated here briefly as a process that would be easy to follow. This list is followed by a more detailed description of each step with further explanations for clarification. The methodology is applied to the data of the research flight of 25 August 2009 over central India (for further information and description of instrumentation see Kulkarni et al., 2009) as an example. Additional examples can be found in the supplementary material online.

1. Assume extreme inhomogeneous mixing. Derive a first estimation for N_a ($N_{a_{init}}$) from the slope of LWC_a to R_v^3 for AF larger than e.g. 0.25 (Fig. 2 and Eq. 1)

2. Use $N_{a_{init}}$ to calculate the relative humidity that the entrained air would have had if it was homogeneously mixed into the cloud (henceforth RH_{best}) for each horizontal cloud penetration. Figure 3a shows an example of how the results typically look.

3. Use the mean RH_{best} for all penetrations that were derived in step 2 to evaluate the effect of inhomogeneous vs. homogeneous mixing on N_a. Then reduce $N_{a_{init}}$ according to this effect (Fig. 4).

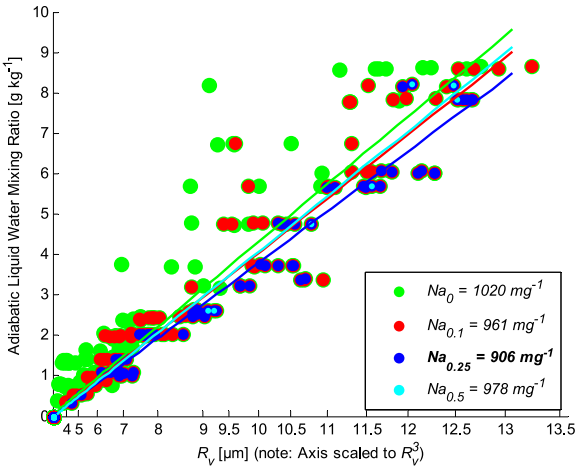

Fig. 2. The droplet mean volume radius (R_v) vs. the adiabatic liquid water mixing ratio (LWC_a) for different threshold adiabatic fractions. The 1 Hz measurements were taken during the CAIPEEX-1 (Cloud-Aerosol Interaction and Precipitation Enhancement Experiment, phase 1; Kulkarni et al., 2009) program over central India on 25 August 2009 (flight 20090825) at elevations between 500 and 5000 m.a.s.l. The green, red, blue and cyan colors denote threshold adiabatic fractions of 0, 0.1, 0.25 and 0.5, respectively. The R_v and AF data are based on the Droplet Measurement Technologies (DMT) Cloud Droplet Probe (CDP) measurements while the number of activated CCN (N_a) is derived from the slope of the linear best fit (Eq. 1). It can be seen that the AF filter selected does not affect the derived N_a remarkably. Using $N_{a_{0.25}}$ as $N_{a_{init}}$ looks like a reasonable compromise between having enough data points to represent the entire profile, and having a large LWC_a range for deriving a representative $N_{a_{init}}$ for the entire profile.

4. Calculate RH_{best} for each penetration again, this time based on the corrected N_a from step 3, similar to what is done in step 2 (Fig. 3). Then calculate the mean penetration residual (MPR).

5. Slightly reduce the last derived N_a (e.g. by 5 %) and repeat steps 4 and 5 until MPR reaches its minimum value (see example in Fig. 3b). The number of iterations for each dataset depends on the amount of N_a reduction chosen for this step.

3.1 Step 1: calculating $N_{a_{init}}$ by assuming extreme inhomogeneous mixing

The liquid water content of a cloud parcel is the sum of masses of all droplets or the product of the droplet number concentration and the mass of a droplet with an average volume, i.e droplet whose radius is R_v. Since all small cloud droplets are spherical N_a can be calculated in the following way:

$$N_a = \frac{1}{\rho_w} \cdot \frac{3}{4\pi} \cdot \frac{LWC_a}{R_{v_a}^3} \quad (1)$$

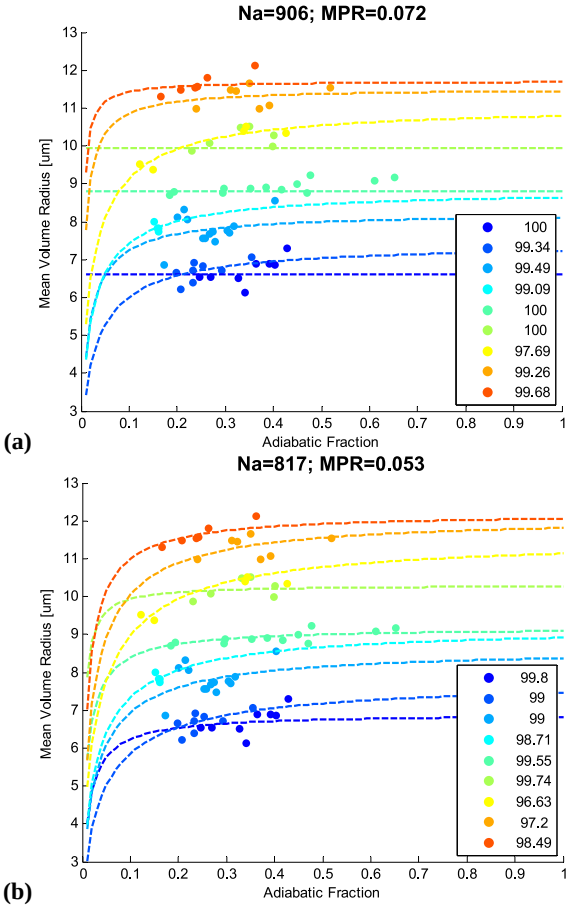

Fig. 3. **(a)** A mixing diagram for different horizontal cloud passes at various altitudes within the same cloud. Each data point is based on the CDP 1 Hz measurement from flight 20090825 (the same as in Fig. 2) and each color denotes the same cloud pass. The dashed lines denote the R_v to AF theoretical relations for the derived RH_{best} (see text for description) that best fits the data points (with AF>0.1) for each cloud pass separately. $N_{a_{init}}$, which is used in the derivation of the RH_{best} values for each penetration (shown in the legend), as well as the mean penetration residual (MPR; see Sect. 3.4) calculated for all fits, are shown at the top of the panel. **(b)** Same as **(a)**, but with the final derived N_a (see Sect. 3.4) and the minimal MRP that showed best overall fit to the same dataset as in panel **(a)**. The legend shows that there is a small decrease in the RH_{best} values in this panel. This is due to the higher R_{v_a} values here in comparison to **(a)**.

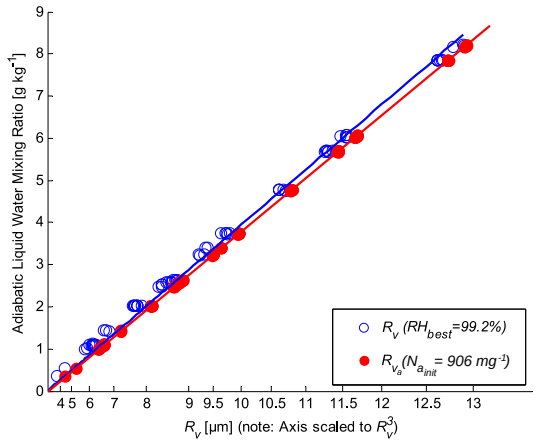

Fig. 4. R_v (blue circles) and R_{v_a} (red circles) vs. the adiabatic liquid water mixing ratio (LWC_a). The red data points denote the calculated R_{v_a} based on the inferred LWC_a profile of flight 20090825 over central India, and $N_{a_{init}}$ (= 906 mg^{-1}) that was derived by Eq. (1) for the data points with AF>0.25 (Fig. 2). The blue data points show the theoretical values of R_v based on the actual 1 Hz AF data (>0.25) and $N_{a_{init}}$, assuming homogeneous mixing with entrained air whose RH_{best} is the mean of the RH_{best} values in Fig. 3a. The ratio of the slopes of the blue and red linear best fits approximates the effect of the homogeneous vs. inhomogeneous mixing assumptions on N_a, and is therefore used as a first correction for $N_{a_{init}}$.

where ρ_w is the water density, which is nearly constant at 1 g cm^{-3}. Because we deal with rising air and change of altitude, all concentration units are per unit mass instead of the more standard volume units. We use [mg^{-1}] and [kg^{-1}] to replace [cm^{-3}] and [m^{-3}] respectively, by multiplying by the air density. The profile of LWC_a is determined by the cloud base pressure and temperature and it indicates the amount of water vapor that turned into cloud water in an adiabatic parcel. N_a can represent the number of activated CCN for the entire profile as long as there is no significant droplet coalescence, as it reduces the droplet number concentration. Because the vast majority of measurements inside a deep convective cloud do not even come near the adiabatic fraction of unity, the challenge is to get a good representation of R_{v_a} based on the measurements of R_v[2], as R_{v_a} strongly affects N_a (Eq. 1).

Freud et al. (2008) showed that R_e is not very sensitive to the degree of mixing in deep convective clouds sampled in the Amazon basin. They concluded therefore that mixing tends towards the inhomogeneous extreme. If this is the case then R_e and R_v anywhere in the cloud are expected to be close to their corresponding adiabatic values, regardless the history of the entrainment and mixing processes in the cloud. Therefore, as a first approximation, we can assume inhomogeneous mixing by using the calculated R_v instead of the theoretical R_{v_a} in Eq. (1). Since ρ_w is nearly constant, N_a can be derived from the mean ratio of LWC_a to $R_{v_a}^3$ (Eq. 1 and Fig. 2).

Figure 2 presents the relationships between R_v^3 and LWC_a for different but overlapping subsets of the 1 Hz data from CAIPEEX-1 (Cloud-Aerosol Interaction and Precipitation

[2]Normally R_e is measured and used rather than R_v. For simplicity and consistency of the description of the methodology we use R_v in the examples. However, in Sect. 3.5 we show how to use R_e with the proposed methodology

Enhancement Experiment, phase 1; Kulkarni et al., 2009) flight 20090825 over central India. Each subset has a different minimum adiabatic fraction threshold, so the datasets become smaller as the threshold increases. The slope of the best fit line of each dataset is used to calculate N_a, which we will henceforth refer to as $N_{a_{init}}$ to point out that this is the first and initial N_a estimation based on the assumption of extreme inhomogeneous mixing. For deriving $N_{a_{init}}$ with Eq. (1), the best fit line has to be forced through the axes-origin. One can see that only few data points have AF>0.5 (the cyan data points), which means that most parts of the cloud are far from adiabatic. There is still a fairly wide range of adiabatic fractions which represents the varying proportions of cloudy and ambient air mixtures. Using various adiabatic fractions as filters (the different colors in Fig. 2) yields slightly different values for the derived $N_{a_{init}}$, depending on the specific dataset. If mixing was indeed extremely inhomogeneous, $N_{a_{init}}$ would not have been dependent on the AF filter whatsoever. However this is clearly not the case and we do see a small decrease in R_v at the smaller adiabatic fractions (green and red markers in Fig. 2), which seemingly affects the derived $N_{a_{init}}$ to some extent. Because we do not have adiabatic samples throughout the vertical profile and we do not know the actual N_a, the adiabatic slope in Fig. 2 is not known. We can though still expect N_a to be lower than $906\,mg^{-1}$, which is the minimal $N_{a_{init}}$ in the presented case. Another added value of using AF as a filter is for excluding data points from adjacent clouds with higher bases that occasionally exist and can not always be evaded when collecting data. These clouds would have smaller R_v in relation to the convective clouds of our interest at the same altitude, so we desire to exclude them from our analysis. The trade off of using a too high AF threshold may be that too many data points will not pass the filter and that the remaining data points may be concentrated at the lower part of the profile, so the derived $N_{a_{init}}$ would be too sensitive to small errors in R_v and LWC_a. Using AF>0.25 as the threshold for calculating $N_{a_{init}}$ (the blue data points and slope in Fig. 2) would be a good compromise. It is important to mention though that the final derivation of N_a is not sensitive to the AF threshold chosen here.

In theory and as shown in Eq. (1), the derived N_a depends on the inferred LWC_a, therefore it is very important to document the cloud base properties (altitude, pressure and temperature) correctly. In fact, if the cloud bases cannot be documented because of e.g. air traffic control limitations or high terrain, the maximum integrated LWC values can assist in estimating the highest possible cloud base altitude, because they cannot exceed the inferred LWC_a values. However, if the cloud base properties are well documented the same condition can be applied to make sure that there is no overestimation of droplet concentration and/or oversizing of the droplets by the cloud droplet probe. Such cases would require corrections of the dataset as they affect the derived N_a (see Sect. 3.6).

3.2 Step 2: using $N_{a_{init}}$ to calculate RH_{best}

$N_{a_{init}}$ derivation is based on the assumption of extreme inhomogeneous mixing. In order to improve the first estimation of N_a, the degree of actual mixing inhomogeneity must be taken into account. This can be done by examining the dependence of R_v on AF (as shown in the theoretical example in Fig. 1) for each horizontal penetration independently. This is not only because R_v is altitude-dependent, but due to the fact that the degree of mixing inhomogeneity may vary with altitude because droplets grow and turbulence changes. The theoretical relative humidity that best fits each penetration-data, RH_{best}, can be found by assuming homogeneous mixing and using the R_v to AF relationship as well as the values of LWC_a and $N_{a_{init}}$. RH_{best} represents the theoretical RH of the entrained air if it were homogeneously mixed with an adiabatic cloud at a specific level (and the number of droplets was conserved). The closer RH_{best} is to the real ambient RH, the stronger the tendency of the mixing towards the homogeneous limit. Figure 3 shows examples of such RH_{best} fits, calculated for horizontal penetrations at varying altitudes as represented by the different colors, for the 20090825 case study. Focusing on the left panel (Fig. 3a); the RH_{best} calculation in this panel uses $N_{a_{init}}$ as input, which determines R_{v_a} for each penetration or level. The mean RH_{best}, as can be derived from the individual RH_{best} values presented in the legend, is smaller than 100 % because R_v is not independent of AF. This is another indication that the mixing is not extremely inhomogeneous.

The mixing diagram (Fig. 1) is based on the assumption that the droplet number remains constant throughout the mixing process (until all droplets evaporate at once), and that no coalescence changes the drop concentration during the process. Significant coalescence does not occur below about R_e of 13 µm (Freud and Rosenfeld, 2011). Therefore samples with R_e>13 µm were excluded from this and the following steps. Using this filter, however, typically does not affect the derived N_a because the vast majority of measurements have R_e <13 µm

3.3 Step 3: correcting $N_{a_{init}}$ by assuming homogeneous mixing

Although $N_{a_{init}}$ is based on the extreme inhomogeneous assumption, still some of the RH_{best} values that were derived in the previous step are smaller than 100 % (Fig. 3a). This implies that mixing is not extremely inhomogeneous and it allows to derive a more realistic N_a than $N_{a_{init}}$. This is done by deriving N_a from the relationship between LWC_a and $R_{v_a}^3$, in a quite similar way to what is shown in Fig. 2, but without assuming extreme inhomogeneous mixing.

The red data points in Fig. 4 denote the R_{v_a} values calculated from $N_{a_{init}}$ and the inferred LWC_a profile. However, since RH_{best} values were already derived in the previous step, we can use their mean value in order to

calculate the theoretical R_v values for the actual AF data (with the same AF filter as used in Fig. 2, i.e. 0.25) without assuming extreme inhomogeneous mixing. This is done by assuming homogeneous mixing with pre-moistened entrained air (with RH = $\overline{\text{RH}}_{\text{best}}$), which appears to be a better representation of reality than assuming extreme inhomogeneous mixing (Burnet and Brenguier, 2007). The blue circles in Fig. 4 denote the derived theoretical R_v values for the actual AF values. The ratio between the blue and red linear best-fit slopes indicates by which factor N_a changes due the assumption of fully homogeneous vs. extreme inhomogeneous mixing, respectively. $N_{a_{init}}$ can therefore be divided by this factor as a first correction towards finding N_a that best fits the dataset. In the example shown in Fig. 4 this factor equals 0.963 while in other cases it can be as low as ∼0.8, depending on $\overline{\text{RH}}_{\text{best}}$. However, this is still not the final and best estimation of N_a, because $\overline{\text{RH}}_{\text{best}}$ was based on $N_{a_{init}}$, which was known a-priori to be an overestimation of the real N_a, but nonetheless this step makes the described methodology more efficient by reducing the number of iterations required in the following steps.

3.4 Steps 4–5: iterations for finding minimal residuals

Because RH_{best} and the estimated N_a depend on each other, N_a derived in step 3 is not necessarily the final one. In order to quantify the quality of the RH_{best} fits, which were derived by prescribing N_a, the mean penetration residual (henceforth MPR) can be calculated for the entire profile. This is done by averaging the squared vertical distance of all data points from the best fit curve in each penetration separately, and then averaging all penetrations, so that each penetration gets the same weight in the averaging regardless of the length of the cloud pass. The lower the MPR the better the overall RH_{best} fits (see MPR values in both panels in Fig. 3 and in the online supporting material).

The aim of the iterations is to find the N_a for which the MPR is minimal. Steps 1–3 brought N_a to a good starting point for the iterations, which can be considered as fine tuning of N_a. N_a should be tuned downwards, because assuming extreme inhomogeneous mixing and hence small R_{v_a}, results in higher N_a (Eq. 1) than without this assumption. A reasonable step for each iteration would be to lower N_a by increments of a few percents, depending on how much we trust the cloud droplet measurements and how certain we are in the cloud base altitude (see Sect. 3.6 for discussion on uncertainties). MRP is computed in each iteration, based on the recalculated RH_{best} fits, until the minimal MPR is found. Smaller increments will result in more iterations. The corresponding N_a to the minimal MPR is the N_a that best fits the entire profile data. This still allows the degree of mixing inhomogeneity to vary with altitude and by penetration. The RH_{best} values for penetrations at different cloud depths has an added value because they can be used to assess the change in the effects of the nature of the entrainment and mixing with altitude, which has rarely been done in the past. But in order to do that there is a need for a more complex mixing model that simulates the changes in the shape of the DSD as well as reliable and accurate profiles of RH outside the clouds and near the cloud edges, which we currently do not possess.

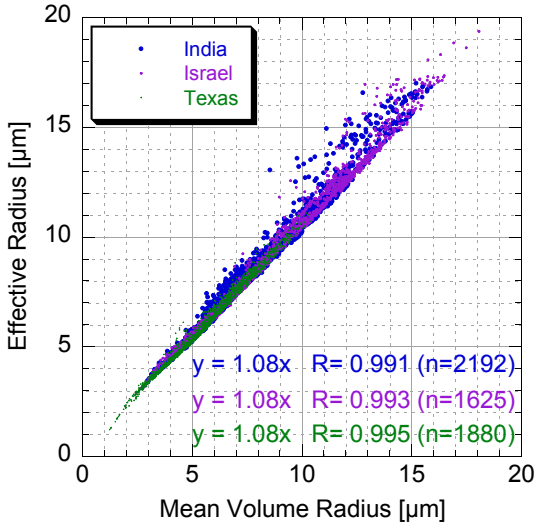

Fig. 5. The cloud droplet effective radius, R_e, versus the droplet mean volume radius, R_v, for over 5800 1Hz-averaged droplet size distributions mainly in convective clouds. The color-coding represents different field campaigns and location data: purple for the Israeli rain enhancement program; blue for CAIPEEX-1 in India; and green for SPECTRA (The Southern Plains Experiment in Cloud seeding of Thunderstorms for Rainfall Augmentation; Axisa et al., 2005). The number of measurements that were used to calculate the linear best-fit for each location is denoted by "*n*" in the lower-right part of the figure. Notice that R_e is larger than R_v on average by 8 % regardless of the location, and that the linear correlation coefficient is greater than 0.99. This means that for practical uses R_e may be used instead of R_v for the derivation of N_a (see Eq. 4).

3.5 Replacing R_v with R_e

The methodology described above uses R_v to derive N_a. However, in remote sensing and in-situ applications normally R_e is measured and used rather than R_v. R_e is always larger than R_v, except for the theoretical case of a monodispersed cloud-droplet population. The ratio between R_e and R_v depends on the specific droplet spectrum, but typically is around ∼1.1 and exhibits little variance because the two variables are highly correlative (Fig. 5).

In order to replace R_v with R_e a new parameter needs to be defined:

$$\alpha = R_e \cdot \left(\frac{N}{\text{LWC}}\right)^{\frac{1}{3}} \quad (2)$$

here N and LWC are the measured droplet concentration and liquid water content, respectively. The physical units of α are

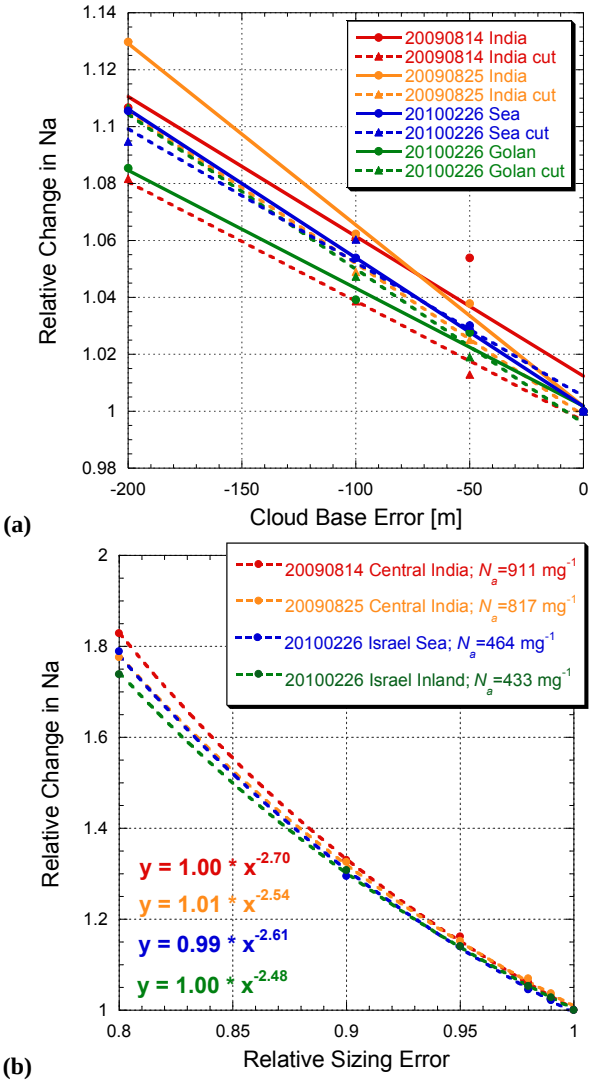

Fig. 6. Sensitivity tests: **(a)** The relative change in N_a due to uncertainties in cloud base altitude for four different cases (flights 20090814 and 20090825 over central India and two profiles from flight 20010226 over Israel, one over the sea and one ∼70 km inland). The change in cloud base altitude causes changes in the cloud base pressure and temperature, and hence modifies the profile of LWC_a. This affects R_{v_a} and AF and eventually N_a. The filled circles and solid linear best fit curves mark that N_a derivation was based on the full profile, while the filled triangles and dashed lines mark that the data from the first kilometer above cloud base were filtered out before N_a was derived. This suggests that when there is no data available from the lower part of the profile, N_a can be derived with the same confidence as when all data is available. **(b)** The relative change in N_a due to uncertainties in the sizing of the cloud droplets by the cloud droplet spectrometer. The same cases as in **(a)** are presented with the derived (original) N_a values for each case in the legend, before the errors were introduced. The dashed lines denote the best power fit for each case and show fairly high sensitivity of the derived N_a to sizing errors.

[m kg$^{-\frac{1}{3}}$], however, if the units of [mg^{-1}], [µm] and [g kg^{-1}] are used for N, R_e and LWC respectively, α gets the units of [µm g$^{-\frac{1}{3}}$]. Combining Eq. (1) for non-adiabatic values with Eq. (2) and using the latter above-mentioned units yields:

$$\alpha = 62.03 \cdot \frac{R_e}{R_v} \tag{3}$$

The parameter α can be calculated for each single droplet spectrum. Sometimes the parameter k is used instead of α for relating R_e and R_v (e.g. Martin et al., 1994)[3]. Eq. (3) also applies for adiabatic parcels, therefore Eq. (1) can be approximated by using a mean α (possibly based on the measurements with the highest AF) this way:

$$N_a = \overline{\alpha}^3 \cdot \frac{LWC_a}{R_{e_a}^3} \tag{4}$$

Now with Eq. (4), N_a can be derived from the vertical profile of R_{e_a} rather than R_{v_a} and the knowledge of the cloud base properties and the mean α. The accuracy of the measurement of R_e by remote sensing of convective clouds, is better than 1 µm according to Zinner et al. (2008). On the other hand, the small scatter of the data points in Fig. 5 as well as the calculated standard error values for each dataset, indicate that the uncertainty in $\overline{\alpha}$ is much smaller than 1 %. Therefore the error due to inaccuracies in $\overline{\alpha}$ are negligible with respect to the instrumental sizing errors.

3.6 Susceptibility of methodology to uncertainties

The methodology discussed here to estimate N_a uses the information regarding the inferred LWC_a profile and the droplet sizes as measured by a research aircraft. The calculation of a representative LWC_a profile depends on proper documentation of the cloud base properties, such as height, temperature and pressure. These may slightly vary in a field of growing convective clouds but the effect of this variability is minimized when analyzing cloud elements higher above the average cloud base. This is one of the main benefits when sampling and analyzing deep profiles. Sometimes there are circumstances which do not allow cloud base measurements, such as air traffic control limitations or high terrain. In those cases the cloud base parameters need to be guessed wisely, by e.g. making sure that the measured LWC do not exceed the inferred LWC_a values. Uncertainties in LWC_a not only affect $N_{a_{init}}$ by changing the slope in Fig. 2, it also affects the values of AF and hence RH_{best} and MPR, and eventually the value of the final N_a. Figure 6a shows the sensitivity of the final derived N_a to changes in cloud base height (and a corresponding change in cloud base pressure and temperature according to a standard atmosphere). It shows that lowering the cloud base by 100 m translates into a decrease of ∼5 % in N_a. It also shows that if we exclude all data from the lowest kilometer of the cloud profile, N_a shows the same sensitivity

[3] k and α are related by: $k = (\frac{62.03}{\alpha})^3$

to uncertainties in cloud base altitude. This is reassuring and indicates that even without proper documentation of cloud base, N_a can still be estimated with a high certainty, at least as long as there is good documentation of the rest of the profile.

Some dynamical variability that leads to varying cloud base updrafts (w) is common in a field of convective clouds. The varying cloud base updrafts between clouds and within a single cloud as well, may nucleate a different number of cloud droplets, even if the aerosol properties are the same. However, as the cloud develops, the turbulent mixing of the air inside the cloud reduces the variability (when disregarding entrainment). In addition, the very weak updrafts do not contribute much to the vertical buildup of the clouds. Therefore, the mean updrafts weighted by their contribution to the cloud volume are what that counts for N_a, as defined here. Our sampling strategy naturally favors the deeper clouds for obtaining profiles of deep convective clouds and hence reduce the variability of the mean cloud base updrafts. Moreover, even if the k exponent is assumed to equal unity in the CCN spectra equation:

$$N_a = c \cdot S^k \quad (5)$$

where S is the super-saturation and c is the number of activated CCN at a super-saturation of 1%, then N_a changes only according to $w^{0.5}$ (Rogers and Yau, 1989). Therefore, for the typically smaller k values, the sensitivity of N_a to w is even smaller. This is why R_v that is measured aloft is not nearly as sensitive to variations in cloud base updrafts as it is to N_a.

Other sources of uncertainty are related to the cloud droplet probe that measures the sizes and concentrations of the cloud droplets (Lance et al., 2010). If the sizing of the droplets is trustworthy then correcting for errors in droplet concentration is straight-forward (see Sect. 4). Any left uncertainties in the droplet concentration would be translated into uncertainties in N_a by a factor of $\sim$0.9 (not shown here). However, any sizing errors of the cloud droplets would be amplified when deriving N_a because of their non-linear relations (Eq. 1). Figure 6b shows that the average changes in N_a due to sizing errors by 1, 2, 5, 10 and 20 % are $\sim$3, 6, 15, 30 and 78 %, respectively. This yields a sensitivity of N_a to the sizing error to the power of ~ -2.6, which is slightly smaller than the exponent of R_v in Eq. (1). It is therefore important to test the sizing calibration of the cloud droplet probe as often as possible during field campaigns in order to minimize the effect of sizing errors on the derived N_a.

It is also important to point out that the final derived N_a does not depend on $N_{a_{init}}$, so using a minimum AF for deriving $N_{a_{init}}$ (in Fig. 2) other than 0.25, may only have an effect on the number of iterations needed before reaching the optimal N_a. Using a too small minimum AF and including data from clouds with higher bases, may result in a mean RH_{best} of 100 % in step 2, which will make step 3 redundant and increase the number of iterations. On the other hand, using a too high AF filter may lead to a too low and unreliable $N_{a_{init}}$ value in case it is based on too few data points from the lower part of the cloud, which could be smaller than the actual N_a. Therefore it is advisable to plot the data as shown in Fig. 2 and choose a proper minimum AF to base $N_{a_{init}}$ on.

Changes in N_a also induce changes in RH_{best}. The example in Fig. 3 shows that in the same dataset when prescribing a smaller N_a the resulting RH_{best} values tend to decrease. This is because R_{v_a} becomes larger. A sensitivity test based on the same four examples as in Fig. 6 (not shown here) reveals that the relative change in the mean RH_{best} is approximately half of the relative change in N_a. That means that RH_{best} is even less sensitive to errors in droplet sizing and cloud base estimation than N_a.

Another important point to emphasize is that the methodology described here is valid as long as the droplet number concentration per unit mass of air in an adiabatic parcel remains nearly constant, i.e. droplets grow mainly by condensation with little coalescence that leads to reduction of droplet concentration, and there is no nucleation of new cloud droplets that would increase it. Nucleation of new droplets by entrained CCN (or those that were not activated near cloud base) can occur in case there is a combination of low droplet concentration and accelerating updrafts. In real clouds it is more likely to occur in highly diluted parts of the clouds, so defining a threshold AF as a filter (e.g. 0.1) can be useful to exclude these cases, as well as those cases with data contamination by clouds with higher bases than the clouds of our interest. In addition, droplet concentration is lowered when droplet coalescence is significant and during rainout, so the mixing diagram may not be valid in these cases, which are advised to be excluded from the analysis.

Adding an error bar to the derived N_a at the end of the routine described in Sect. 3 is not an easy task. This is because it mainly depends on the calibration and performance of the specific cloud droplet probe. An advantage is that the routine relies more on the sizing accuracy of the probe rather than on the concentration measurements. Testing the sizing calibration with a spinning disc or by releasing glass beads across the probe laser beam is something that is normally done quite often during a field campaign. The accuracy of a properly calibrated cloud droplet probe is typically higher than the resolution of the probe, i.e. approximately ± 1 µm. Our experience shows that drift in the concentration calibration is more common, therefore it is important to correct this drift in the data analysis phase by e.g. comparing the cloud droplet probe integrated LWC with the Hot Wire LWC, which is usually more reliable as the measurement is quite straight forward in comparison with the cloud droplet probe. Then the droplet concentration could be multiplied by the calculated correction factor, which may change even during flight, while leaving the shape of the droplet size distribution unchanged. Another key point for minimizing uncertainty in N_a estimation, is to avoid mixing clouds with bases at different altitudes or with varying aerosol or thermodynamic properties in the same analysis. Such cases would cause a fairly

large variation in R_v (or R_e) for given LWC_a values, which are calculated for the main cloud base. In order to exclude data from penetrations to clouds with elevated bases, a filter based on a minimum adiabatic fraction could be used (like in the example shown in Fig. 2). Furthermore, penetrations with well developed warm rain or ice formation should also be excluded from the analysis as large fraction of the drops are lost to hydrometeors and the spectra of the remaining drops are altered, hence changing R_e, R_v and AF and consequently the derived N_a. This can be done by e.g. excluding measurements with $R_e > 13\,\mu m$, which normally indicates effective coalescence (Freud and Rosenfeld, 2011), and/or by using the precipitation probe measurements. But because the vast majority of the measurements in each profile have smaller R_e values than 13 µm, the derived N_a is typically not sensitive to whether this filter was applied or not. Some coalescence may also take place at smaller R_e values but the limited time and the partial droplet evaporation due to ongoing mixing help to constrain the variations in R_e.

If these requirements are satisfied, and the steps described in Sect. 3 are followed, the derived N_a is expected to represent quite well the number of activated CCN near the cloud base or even the bases of a field of microphysically similar clouds.

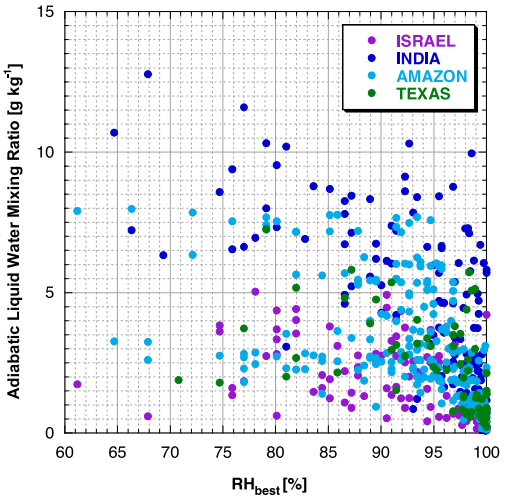

Fig. 7. Each data point represents RH_{best} that was calculated for one cloud pass (and based on the derived N_a of each profile) vs. LWC_a, which relates to the vertical dimension. The same color-coding as in Fig. 5 is used with the addition of data from the Large-Scale Biosphere-Atmosphere Experiment in Amazonia – Smoke, Aerosols, Clouds, Rainfall, and Climate (SMOCC; Andreae et al., 2004) in cyan. It appears like the highest RH_{best} values are found near cloud base, indicating strong tendency towards extreme inhomogeneous mixing, maybe due to the small droplets and fairly weak turbulence there.

4 Results and discussion

We applied the methodology described in the previous section to data collected in deep convective clouds over Israel, India, the Amazon, Texas and California, under a variety of meteorological conditions and aerosol characteristics. N_a was derived for each cloud profile (the profiling was not Lagrangian, but rather penetrating tops of consecutively growing convective clouds in a cloud cluster) and it ranged between 100 to 2500 per milligram of air, which occupies a volume of approximately 1 cm^3 at a typical cloud base altitude of 1.5 km a.s.l.

In the previous section we stated that coalescence becomes active and drizzle particles start to form when R_e reaches ~13 µm. This does not mean that no droplet coalescence takes place at smaller R_e values, but the time is expected to be a limiting factor to droplet growth in convective clouds at small R_e values (Freud and Rosenfeld, 2011). Suppose that we have two clouds with the same N_a. One cloud grows very fast (strong updrafts) and the other grows at a much slower rate. Both eventually reach $R_e = 13\,\mu m$. If time would play a major role in the advancement of coalescence in clouds with $R_e < 13\,\mu m$, the cloud that grows more slowly would have reached 13 µm at much lower altitude. This is not observed to happen, because R_e shows little variation at a given height (e.g. Fig. 5 in Freud and Rosenfeld (2011) and Fig. 3 here), which is explained mainly by the inhomogeneity of the mixing. In addition, a closer look at Fig. 5 shows that the ratio between R_v and R_e becomes more variable when R_e exceeds 13 µm. This indicates that at $R_e < 13\,\mu m$ droplets mainly grow by condensation which maintains the shape of the DSD. Only when droplet coalescence becomes sufficiently active (at $R_e > 13\,\mu m$) the shape of the DSD may change by forming a tail of larger droplets, depending on the droplet concentrations and the available time for droplet coalescence. This would make the R_v to R_e ratio somewhat sensitive to the updrafts.

In addition, the coalescence rate increases linearly with the cloud drop concentration for a given R_e. Therefore, greater AF is expected to cause precipitation initiation at smaller R_e. But we see no obvious evidence for that. We hypothesize that this is because the higher adiabatic fractions are associated with stronger updrafts, leaving less time for coalescence to advance with respect to samples with weaker updrafts and smaller AF. This might serve as a compensating mechanism for the effect of AF on rain initiation, leading to the robustness of the dependence of R_e on cloud depth. It would be interesting look into this hypothesis with a multi-dimensional cloud model that explicitly resolves DSD and entrainment-mixing.

At the end of Sect. 2 we mentioned that the RH of the ambient air together with what we defined in Sect. 3 as RH_{best}, can be used to assess the degree of mixing inhomogeneity. Unfortunately we do not have accurate and reliable RH data, but analyzing the derived RH_{best} values for many penetrations can still be informative. Figure 7 shows the derived

RH_{best} values of more than 500 penetrations in convective clouds over Israel, India, the Amazon and Texas, versus the adiabatic liquid water mixing ratio for each penetration, which is a representation of the vertical dimension. There is a fair amount of scatter in the data, but the median RH_{best} is 95.25 %. This value is definitely higher than the typical RH aloft between the convective clouds, and therefore an indication that in the vast majority of cases, the entrainment-mixing process is far from fully homogeneous. A closer look on RH_{best} in the vertical dimension may give the impression that there is a weak tendency towards smaller RH_{best} values at larger cloud depths or at least that the highest RH_{best} occurrences are concentrated near cloud base. This may be interpreted as a weak tendency towards homogeneous mixing at greater altitudes, as Small and Chuang (2010) reported in their study based on few cases, but by using slightly different methods. A possible explanation for this trend is that turbulence aloft is more pronounced due to stronger updrafts aloft, so τ_{mix} decreases. In addition the droplets are larger aloft so τ_{evap} increases for a given RH. This results in a decrease in the Damköhler ratio and hence a tendency towards homogeneous mixing aloft. Since we do not have accurate profiles of ambient RH in the cloud-free air, our dataset does not enable us to rule out that all apparent RH_{best} decrease aloft can be explained by lower ambient RH at greater altitudes, which is not uncommon in an unstable atmosphere with convective clouds. But even if there were such RH measurements, most entrained air comes from the direct vicinity of the clouds. This air may be more humid due to the evaporated cloud droplets and may produce humidity halos around the clouds (e.g. Lu et al., 2003; Heus and Jonker, 2008). However, measuring accurately the small changes in RH by a fast moving aircraft is very challenging.

Moreover, in the simple model results shown in Fig. 1, as in earlier publications, the mixing of entrained air is assumed to occur with an adiabatic parcel at a constant level. This is of course not necessarily true, as different parcels in the clouds may have been exposed earlier to entrained air at other altitudes. In convective clouds, the air can move vertically quite rapidly, so if a mixing event at a low altitude already caused a small reduction in R_v, and another mixing event higher up caused an additional small reduction in R_v, the combined effect will result in a smaller derived RH_{best} than when we assume exclusive one-level mixing. This is because in one-level mixing the maximal R_v is always R_{v_a} while in secondary mixing even if it is extremely inhomogeneous, R_v would be smaller than R_{v_a} and RH_{best} would be under-estimated. This might cause a false interpretation of a trend towards homogeneous mixing aloft and may partly contribute to the tendency seen in Fig. 7. In addition, the preferential evaporation of the smaller droplets, which is not accounted for in the simple homogeneous mixing model, adds complexity and uncertainty, and requires a deeper analysis with detailed simulations. Therefore we cannot say that we found proof for clear tendency towards less inhomogeneous mixing higher in the cloud, but clearly mixing has a general tendency towards the inhomogeneous limit at all levels as indicated by the high RH_{best} values.

Our interpretation of the high RH_{best} values is that the entrained drier air quickly causes a total evaporation of the cloud droplets that border the entrained parcel, so the entrained air gets more moist but cannot be considered as a cloud at that point. As it approaches saturation, the molecular diffusion of vapor from the droplets to the sub-saturated air slows down, increasing the time scale of the droplet evaporation, so further turbulent mixing with the cloud tends to be more homogeneous. It appears that the entrained air is pre-moistened (this term has been used by Burnet and Brenguier, 2007) in a nearly extreme inhomogeneous manner and then is mixed more homogeneously as it approaches saturation. Small and Chuang (2010) compared edges and cores of clouds and found a similar tendency. At smaller scales than that is measured with a 1 Hz probe on an aircraft ($\sim$100 m), mixing may have an increased tendency toward the homogeneous mixing type (Lehmann et al., 2009), but variations in such scales cannot be resolved with our current dataset. However, for applications requiring spatial resolutions of $\sim$100 m and above, the mixing can be considered as highly inhomogeneous.

As discussed in Sect. 3, taking into account the mixing inhomogeneity is important for obtaining a better estimation for N_a. The example in Fig. 3 shows that using the final N_a (panel b), as compared to $N_{a_{init}}$ (panel a) that is based on the extreme inhomogeneous mixing assumption, results in improved overall fits of the RH_{best} curves to the data points. This example is not unique, we find similar improvements in all analyzed profiles (see more examples in the supplementary online material). The difference between N_a and $N_{a_{init}}$ is on average $\sim$30 %, as Fig. 8 shows, regardless of location. This means that it is important to account for the relative inhomogeneity of the mixing at all levels despite the high median RH_{best} (95.25 %), which clearly indicates a strong tendency towards the extreme inhomogeneous mixing limit. What is also evident in Fig. 8 is that all data points fall above the 1:1 dashed line. This is because the inhomogeneous mixing assumption, which is made to derive $N_{a_{init}}$, marks the upper limit of the N_a estimation. If the actual mixing is more inhomogeneous, then the difference between N_a and $N_{a_{init}}$ would be less pronounced.

N_a, being an estimation of the number of activated CCN near the cloud base, can be compared against the CCN concentrations at a given super-saturation that were measured below cloud base. This may reveal some information about the CCN activation process and/or instrument performance. Such a comparison is shown Fig. 9. This plot displays data from different locations, instruments and super-saturations, as indicated in the figure legend. A perfect fit between the CCN concentration at a given super-saturation and N_a should not be expected because N_a encapsulates the information about cloud base updrafts, which the CCN concentration is

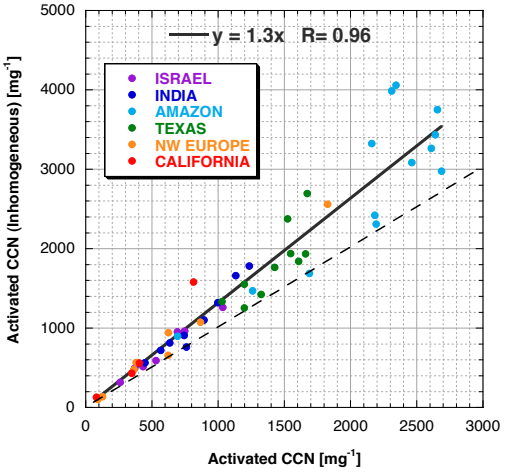

Fig. 8. Comparison of $N_{a_{init}}$, which is based on extreme inhomogeneous mixing assumption, with the final derived N_a, that assumes homogeneous mixing with pre-moistened air. The color-coding is the same as in Fig. 7, with added data from flights within the projects of EUCAARI (European Integrated project on Aerosol Cloud Climate and Air Quality interactions; Kulmala et al., 2009) over the Netherlands and the North Sea (in orange) and SUPRECIP (Suppression of Precipitation Experiment; Rosenfeld et al., 2008b) over California (in red). Each data point here represents one profile. The black linear best-fit and equation show that, on average, N_a is smaller than $N_{a_{init}}$ by ~30 %. It does not appear like there are significant differences between the different locations, as they fall within the same range of slopes, although the Amazon and Texas data stand out for having generally high and maybe slightly unreasonable values of N_a, which may be an indication of droplet undersizing by the cloud droplet probes (see Sect. 3.6).

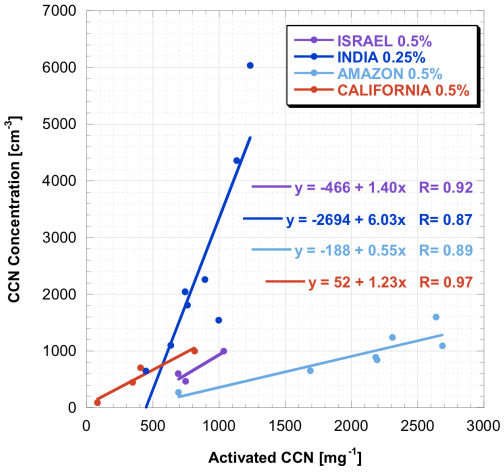

Fig. 9. CCN concentration vs. N_a. Each data point denote a full vertical profile in a deep convective cloud. The CCN concentrations were measured below cloud base (with DMT CCN counters) at different super-saturations as indicated in the legend. The color-coding is similar to Figs. 7 and 8 and represents the different field campaigns. Notice the fairly strong linear relationship in each field campaign separately. The different slopes cannot be fully explained by differing updrafts and super-saturations, but rather by the different instruments and calibrations used.

independent of. Despite that, the linear fit for each location separately, shown in Fig. 9, is fairly good (R>0.87), but the different locations exhibit significantly different slopes. This is probably due to the different instrumentation and calibrations used in each location and optionally different cloud base updrafts. Taking into account the characteristic cloud base updraft speed (Morales and Nenes, 2010) may help explaining some of the differences between the locations. However the relatively small variability around the fit within a location indicates that the variability in updrafts cannot explain the very different slopes. This would be mainly caused by the cloud drop spectrometer sizing and counting errors, as well as the different calibrations of the CCN counters. If the cloud droplet probe is calibrated properly and performs well, the N_a to CCN relationship can be used to roughly estimate the characteristic cloud base updraft, providing that the CCN spectra is known. That would be one example of an applicable use of N_a.

Another interesting finding which may be applicable, is that N_a was not very sensitive to small variations in cloud base altitude and did not differ significantly when the lower part of the cloud profile was not considered. This is because the N_a derivation utilizes information from different levels, and the error in fractional adiabatic water becomes smaller at greater cloud depths. This renders this methodology especially suitable for remote-sensing derivations, which normally do not "see" the lowest parts of the convective clouds.

5 Summary and conclusions

The study presented here aims at deriving the number of activated CCN into cloud droplets near cloud base in deep convective clouds. These clouds are prone to significant mixing with entrained dry air, due to their relatively small horizontal extent, strong turbulence and the fact that they tend to grow into sub-saturated layers of air. Here we present a methodology for deriving N_a from data of substantially sub-adiabatic clouds, by first assuming that the entrainment and mixing of air into the cloud is extremely inhomogeneous. This yields the upper limit for N_a, which we refer to as $N_{a_{init}}$ and that serves as a starting point for the fine tuning of the final N_a derivation as well as to obtain information regarding the nature of the mixing process between the cloudy and the entrained sub-saturated ambient air.

The N_a derivation methodology regards the cloud, or set of clouds, as a unity, so N_a is more like a macro-physical property of the cloud or the cloudy domain, as long as the aerosol properties and thermodynamics are fairly homogeneous. N_a represents the typical number concentration of CCN that are activated into cloud droplets near the bases of

the measured cloud or cloud cluster. It is initially based on the entire profile data and then tuned based on data of individual cloud penetrations. N_a is independent of the actual amount of entrainment aloft, which can vary significantly between clouds. In order to apply this methodology it is necessary to penetrate convective clouds at different levels. Preferably in horizontal penetrations from cloud base to the level where significant precipitation is formed (i.e. not precipitation falling from above). Significant precipitation for that matter means that more than a few percent of the cloud water, as measured by a precipitation probe, has been converted into hydro-meteors (e.g. Freud and Rosenfeld, 2011). The described methodology may also be applied to shallow convective clouds, but the confidence in the derived N_a may be slightly reduced due to potential increase in N_a sensitivity to sizing errors of the cloud droplet probe and small variations/errors in cloud base properties (Sect. 3.6). Applying the methodology to stratiform clouds is typically not as advantageous compared to the methods that have been used already for such clouds (e.g. Bennartz, 2007) because nearly adiabatic cloud parcels, in which droplet concentrations are essentially N_a, are very common.

After applying the methodology described in Sect. 3 to a large set of data collected in Israel, India, the Amazon, Northwestern Europe, Texas and California, we conclude the following:

- R_v^3 (and R_e^3) grows nearly linearly with the adiabatic water mixing ratio in deep convective clouds before significant droplet coalescence takes place, at a rate that primarily depends on N_a.
- N_a is closely related to the CCN concentrations. Characteristic updrafts and cloud base super-saturations may be derived from this relationship and the measured CCN activation spectra.
- Mixing of sub-saturated air into the cloud according to our dataset and spatial resolution appears to be strongly inhomogeneous, but does not reach the extreme inhomogeneous limit. The results presented here support the thesis that the entrained air is pre-moistened by quickly evaporating cloud droplets at first and then mixes more homogeneously as it approaches saturation.
- It appears like mixing may be less inhomogeneous higher in the cloud due to the larger cloud droplets and stronger turbulence there. Drier air aloft and the history of mixing at lower levels of the cloud may also contribute the this observed trend.

Supplement related to this article is available online at: http://www.atmos-chem-phys.net/11/12887/2011/acp-11-12887-2011-supplement.pdf.

Acknowledgements. Some of the examples presented in this paper rely in parts on data obtained from the Cloud Aerosol Interaction and Precipitation Enhancement Experiment (CAIPEEX) of the Indian Institute of Tropical Meteorology (IITM), with J. R. Kulkarni as a program manager and B. N. Goswami as the director. Additional examples are based on data from Texas, with D. Axisa having taken the lead on the instrumented aircraft, data collection and quality control. Some additional aircraft data are taken from the European Integrated Project on Aerosol Cloud Climate Air Quality Interactions (EUCAARI) in northwestern Europe, and from the Smoke Aerosols, Clouds, Rainfall and Climate (SMOCC) aircraft campaign in the Amazon. Both EUCAARI and SMOCC were funded by the European Commission. Data are used also from the research flights of the Israeli rain enhancement program funded by the Israeli Water Authority, and from the SUPRECIP campaign in California, funded by the California Energy Commission. The authors would like to express their gratitude to all sponsors, partners and collaborators for their efforts in collecting these valuable and extensive datasets.

Edited by: A. Nenes

References

Albrecht, B. A.: Aerosols, Cloud Microphysics and Fractional Cloudines, Science, 245, 1227–1230, 1989.

Andreae, M., Rosenfeld, D., Artaxo, P., Costa, A., Frank, G., Longo, K., and Silva-Dias, M.: Smoking rain clouds over the Amazon, Science, 303, 1337, doi:10.1126/science.1092779, 2004.

Andreae, M. O.: Correlation between cloud condensation nuclei concentration and aerosol optical thickness in remote and polluted regions, Atmos. Chem. Phys., 9, 543–556, doi:10.5194/acp-9-543-2009, 2009.

Axisa, D., Rosenfeld, D., Santrpia, J., Woodley, W., and Collins, D.: The Southern Plains Experiment in Cloud Seeding of Thunderstorms for Rainfall Augmentation (SPECTRA) Project: Operational tools used towards verifying glaciogenic and hygroscopic seeding conceptual models, case studies and preliminary results, in: 16th Conference on Planned and Inadvertent Weather Modification, 2005.

Baker, M. B., Corbin, R. G., and Latham, J.: The Influence of entrainment on the evolution of cloud droplet spectra. 1. A model of inhomogeneous mixing, Q. J. Roy. Meteorol. Soc., 106, 581–598, 1980.

Baker, M. B., Breidenthal, R. E., Choularton, T. W., and Latham, J.: The Effects of Turbulent Mixing in Clouds, J. Atmos. Sci., 41, 299–304, 1984.

Barahona, D. and Nenes, A.: Parameterization of cloud droplet formation in large scale models: including effects of entrainment, J. Geophys. Res., 112, D16206, doi:10.1029/2007JD008473, 2007.

Bennartz, R.: Global assessment of marine boundary layer cloud droplet number concentration from satellite, J. Geophys. Res, 112, D02201, doi:10.1029/2006JD007547, 2007.

Blyth, A. M., Choularton, T. W., Fullarton, G., Latham, J., Mill, C. S., Smith, M. H., and Stromberg, I. M.: The Influence of entrainment on the evolution of cloud droplet spectra. 2. Field experiments at Great Dun Fell, Q. J. Roy. Meteorol. Soc., 106, 821–840, 1980.

Bower, K. and Choularton, T.: The effects of entrainment on the growth of droplets in continental cumulus clouds, Q. J. Roy. Meteorol. Soc., 114, 1411–1434, 1988.

Brenguier, J. L.: Observations of Cloud Microstructure at the Centimeter Scale, J. Appl. Meteorol., 32, 783–793, 1993.

Brenguier, J. L., Pawlowska, H., Schuller, L., Preusker, R., Fischer, J., and Fouquart, Y.: Radiative properties of boundary layer clouds: Droplet effective radius versus number concentration, J. Atmos. Sci., 57, 803–821, 2000.

Burnet, F. and Brenguier, J. L.: Observational study of the entrainment-mixing process in warm convective clouds, J. Atmos. Sci., 64, 1995–2011, 2007.

Dimotakis, P. E.: Turbulent mixing, Ann. Rev. Fluid Mech., 37, 329–356, 2005.

Freud, E. and Rosenfeld, D.: Linear relation between convective cloud drop number concentration and depth for rain initiation, J. Geophys. Res., doi:10.1029/2011JD016457, in preparation, 2011.

Freud, E., Rosenfeld, D., Andreae, M., Costa, A., and Artaxo, P.: Robust relations between CCN and the vertical evolution of cloud drop size distribution in deep convective clouds, Atmos. Chem. Phys, 8, 1661–1675, doi:10.5194/acp-8-1661-2008, 2008.

Gerber, H.: Entrainment, mixing, and microphysics in RICO cumulus, in: Proc. 12th Conf. On Cloud Physics, 2006.

Heus, T. and Jonker, H.: Subsiding shells around shallow cumulus clouds, J. Atmos. Sci., 65, 1003–1018, 2008.

Hill, T. and Choularton, T.: An airborne study of the microphysical structure of cumulus clouds, Q. J. Roy. Meteorol. Soc., 111, 517–544, 1985.

IPCC: Climate Change 2007 – The Physical Science Basis, Contribution of Working Group 1 to the Fourth Assessment Report of the Intergovernmental Panel on Climate Change, Cambridge University Press, Cambridge, UK and New York, 2007.

Jensen, J. and Baker, M.: A Simple Model of Droplet Spectral Evolution during Turbulent Mixing., J. Atmos. Sci., 46, 2812–2829, 1989.

Koren, I., Remer, L., Altaratz, O., Martins, J., and Davidi, A.: Aerosol-induced changes of convective cloud anvils produce strong climate warming, Atmos. Chem. Phys, 10, 5001–5010, doi:10.5194/acp-10-5001-2010, 2010.

Kulkarni, J., Maheskumar, R., Konwar, M., Deshpande, C., Morwal, S., Padma Kumari, B., Joshi, R., Pandithurai, G., Bhalwankar, R., Mujumdar, V., et al.: The Cloud Aerosol Interactions and Precipitation Enhancement Experiment (CAIPEEX): overview and prominent results, in: AGU Fall Meeting Abstracts, vol. 1, p. 1, 2009.

Kulmala, M., Asmi, A., Lappalainen, H., Carslaw, K., Pöschl, U., Baltensperger, U., Hov, Ø., Brenquier, J., Pandis, S., Facchini, M., et al.: Introduction: European Integrated Project on Aerosol Cloud Climate and Air Quality interactions (EUCAARI) – integrating aerosol research from nano to global scales, Atmos. Chem. Phys., 9, 2825–2841, doi:10.5194/acp-9-2825-2009, 2009.

Lance, S., Brock, C., Rogers, D., and Gordon, J.: Water droplet calibration of the Cloud Droplet Probe (CDP) and in-flight performance in liquid, ice and mixed-phase clouds during ARCPAC, Atmos. Meas. Techn., 3, 1683–1706, doi:10.5194/amt-3-1683-2010, 2010.

Latham, J. and Reed, R. L.: Laboratory studies of effects of mixing on evolution of cloud droplet spectra, Q. J. Roy. Meteorol. Soc., 103, 297–306, 1977.

Lehmann, K., Siebert, H., and Shaw, R. A.: Homogeneous and Inhomogeneous Mixing in Cumulus Clouds: Dependence on Local Turbulence Structure, J. Atmos. Sci. 66, 3641–3659, 2009.

Lu, M., Wang, J., Freedman, A., Jonsson, H., Flagan, R., McClatchey, R., and Seinfeld, J.: Analysis of humidity halos around trade wind cumulus clouds, J. Atmos. Sci., 60, 1041–1059, 2003.

Martin, G., Johnson, D., and Spice, A.: The Measurement and Parameterization of Effective Radius of Droplets in Warm Stratocumulus Clouds, J. Atmos. Sci., 51, 1823–1842, 1994.

Morales, R. and Nenes, A.: Characteristic updrafts for computing distribution-averaged cloud droplet number and stratocumulus cloud properties, J. Geophys. Res, 115, D18220, doi:10.1029/2009JD013233, 2010.

Morales, R., Nenes, A., Jonsson, H., Flagan, R., and Seinfeld, J.: Evaluation of an entraining droplet activation parameterization using in situ cloud data, J. Geophys. Res., 116, D15205, doi:10.1029/2010JD015324, 2011.

Paluch, I.: Mixing and the Cloud Droplet Size Spectrum: Generalizations from the CCOPE Data., J. Atmos. Sci., 43, 1984–1993, 1986.

Paluch, I. and Baumgardner, D.: Entrainment and fine-scale mixing in a continental convective cloud, J. Atmos. Sci., 46, 261–278, 1989.

Pawlowska, H., Brenguier, J. L., and Burnet, F.: Microphysical properties of stratocumulus clouds, Atmos. Res., 55, 15–33, 2000.

Rogers, R. and Yau, M.: A short course in cloud physics, Pergamon, 113, pp. 81-98, 1989.

Rosenfeld, D., Lohmann, U., Raga, G. B., O'Dowd, C. D., Kulmala, M., Fuzzi, S., Reissell, A., and Andreae, M. O.: Flood or drought: How do aerosols affect precipitation?, Science, 321, 1309–1313, 2008a.

Rosenfeld, D., Woodley, W., Axisa, D., Freud, E., Hudson, J., and Givati, A.: Aircraft measurements of the impacts of pollution aerosols on clouds and precipitation over the Sierra Nevada, J. Geophys. Res, 113, D15203, doi:10.1029/2007JD009544, 2008b.

Schüller, L., Brenguier, J., and Pawlowska, H.: Retrieval of microphysical, geometrical, and radiative properties of marine stratocumulus from remote sensing, J. Geophys. Res., 108, 8631, doi:10.1029/2002JD002680, 2003.

Small, J. D. and Chuang, P. Y.: An analysis of entrainment mixing processes in warm cumulus, in: 13th Conference on Cloud Physics, American Meteorological Society, Portland, OR, 2010.

Snider, J. R., Leon, D., and Wang, Z.: Cloud droplet number concentration in VOCALS-REx, in: 13th Conference on Cloud Physics, American Meteorological Society, Portland, OR, USA, 2010.

Twomey, S.: Pollution and Planetary Albedo, Atmos. Environ., 8, 1251–1256, 1974.

Zinner, T., Marshak, A., Lang, S., Martins, J., and Mayer, B.: Remote sensing of cloud sides of deep convection: towards a three-dimensional retrieval of cloud particle size profiles, Atmos. Chem. Phys, 8, 4741–4757, doi:10.5194/acp-8-4741-2008, 2008.